



## Tropospheric ozone radiative forcing uncertainty due to pre-industrial fire and biogenic emissions

Matthew J. Rowlinson<sup>1</sup>, Alexandru Rap<sup>1</sup>, Douglas S. Hamilton<sup>2</sup>, Richard J. Pope<sup>1,3</sup>, Stijn Hantson<sup>4,5</sup>,  
5 Stephen R. Arnold<sup>1</sup>, Jed O. Kaplan<sup>6,7,8</sup>, Almut Arneth<sup>4</sup>, Martyn P. Chipperfield<sup>1,3</sup>, Piers M. Forster<sup>9</sup>, Lars  
Nieradzik<sup>10</sup>

<sup>1</sup>Institute for Climate and Atmospheric Science, School of Earth and Environment, University of Leeds, Leeds, LS2 9JT, UK.

<sup>2</sup>Department of Earth and Atmospheric Science, Cornell University, Ithaca 14853 NY, USA.

<sup>3</sup>National Centre for Earth Observation, University of Leeds, Leeds, LS2 9JT, UK.

10 <sup>4</sup>Atmospheric Environmental Research, Institute of Meteorology and Climate research,  
Karlsruhe Institute of Technology, 82467 Garmisch-Partenkirchen, Germany.

<sup>5</sup>Geospatial Data Solutions Center, University of California Irvine, California 92697, USA.

<sup>6</sup>ARVE Research SARL, Pully 1009, Switzerland.

<sup>7</sup>Environmental Change Institute, School of Geography and the Environment, University of Oxford, Oxford OX1 3QY, UK.

15 <sup>8</sup>Max Planck Institute for the Science of Human History, Jena 07745, Germany.

<sup>9</sup>Priestley International Centre for Climate, University of Leeds, LS2 9JT, Leeds, UK.

<sup>10</sup>Institute for Physical Geography and Ecosystem Sciences, Lund University, Lund S-223 62, Sweden.

Corresponding authors: Matthew J. Rowlinson (ee11mr@leeds.ac.uk); Alex Rap (a.rap@leeds.ac.uk)



**Abstract** Tropospheric ozone concentrations are sensitive to natural emissions of precursor compounds. In contrast to existing assumptions, recent evidence indicates that terrestrial vegetation emissions in the pre-industrial were larger than in the present-day. We use a chemical transport model and a radiative transfer model to show that revised inventories of pre-industrial fire and biogenic emissions lead to an increase in simulated pre-industrial ozone concentrations, decreasing the estimated pre-industrial to present-day tropospheric ozone radiative forcing of up to 34% ( $0.38 \text{ Wm}^{-2}$  to  $0.25 \text{ Wm}^{-2}$ ). We find that this change is sensitive to employing biomass burning and biogenic emissions inventories based on matching vegetation patterns, as co-location of emission sources enhances the effect on ozone formation. Our forcing estimates are at the lower end of existing uncertainty range estimates ( $0.2 - 0.6 \text{ Wm}^{-2}$ ), without accounting for other sources of uncertainty. Thus, future work should focus on reassessing the uncertainty range of tropospheric ozone radiative forcing.

30



## 1 Introduction

Tropospheric ozone ( $O_3$ ) is a short-lived greenhouse gas formed in the atmosphere through photochemical oxidation of volatile organic compounds (VOCs) in the presence of nitrogen oxides ( $NO_x$ ). These precursor gases have both natural and anthropogenic sources, and increased anthropogenic emissions are thought to have caused an increase in global tropospheric  $O_3$  of 25-50% since 1900 (Lamarque et al., 2010; Gauss et al., 2006; Young et al., 2013). The Intergovernmental Panel on Climate Change (IPCC) current best estimate for tropospheric  $O_3$  radiative forcing (RF) over the industrial era is  $0.4 \pm 0.2$   $Wm^{-2}$  with a 5%-95% confidence interval, making tropospheric  $O_3$  the third most important anthropogenic greenhouse gas after  $CO_2$  and  $CH_4$  (Myhre et al., 2013). The present-day (PD) radiative effect (RE) of tropospheric  $O_3$  is relatively well constrained (Rap et al., 2015). The large uncertainty range ( $0.2$ - $0.6$   $Wm^{-2}$ ) is caused by a number of factors such as the radiative transfer scheme employed, the model used to simulate tropospheric  $O_3$  and tropopause definition, however it is primarily associated with a poor understanding of pre-industrial (PI)  $O_3$  concentrations (Myhre et al., 2013; Stevenson et al., 2013). Although measurements of tropospheric  $O_3$  exist as far back as the late 19<sup>th</sup> century, there are limited reliable quantitative measurements of tropospheric  $O_3$  prior to the 1970s (Volz and Kley, 1988; Cooper et al., 2014). Recently Checa-Garcia et al. (2018) found that differences in PI estimates between Coupled Model Intercomparison Project phase 5 (CMIP5) and CMIP6 cause an 8-12% variation in  $O_3$  RF estimates, but did not explicitly assess uncertainty in natural PI emissions. Recent analysis of oxygen isotopes in polar ice cores indicates that tropospheric  $O_3$  in the northern hemisphere increased by less than 40% between 1850 and 2005, indicating that  $O_3$  RF may be lower than the  $0.4$   $Wm^{-2}$  estimate (Yeung et al., 2019).

As well as anthropogenic sources,  $O_3$  precursor gases such as methane ( $CH_4$ ), carbon monoxide (CO) and  $NO_x$  have natural emission sources, e.g., wildfires, wetlands, lightning and biogenic emissions. Wildfires, for example, emit large quantities of CO,  $NO_x$ ,  $CH_4$  and non-methane volatile organic compounds (NMVOCs) (van der Werf et al., 2010; Voulgarakis and Field, 2015), which influence the chemical production of  $O_3$  (Wild, 2007). Changes in the natural environment therefore influence the concentration and distribution of tropospheric  $O_3$  (Monks et al., 2015; Hollaway et al., 2017). However, the human impact on natural emissions over the industrial era is more uncertain than on anthropogenic emissions (Arneth et al., 2010; Mickley et al., 2001). An accurate representation of PI fire occurrence is required for PI to PD tropospheric  $O_3$  RF calculations.

Recent studies suggest that the relationship between humans and fire (Bowman et al., 2009) is more complex than previously assumed (Doerr and Santín, 2016). The expansion of agriculture and land-cover fragmentation since PI has decreased the abundance and continuity of fuel, inhibiting fire spread (Swetnam et al., 2016; Marlon et al., 2008) and hence total emissions. Furthermore at the global scale, increased population density results in declining fire frequency (Knorr et al., 2014; Andela et al., 2017). Increased agricultural land coupled with active fire suppression and management policies mean that human activity has likely caused total fire emissions to decline since the PI (Marlon et al., 2016; Hamilton et al., 2018; Daniau et al., 2012). Paleoenvironmental archives of fire activity also reflect a decline of fire over the industrial era in many regions (Swetnam et



al., 2016; Rubino et al., 2016; Marlon et al., 2016). This change in understanding of PI fire emissions has been shown to have a strong influence on aerosol RF: Hamilton et al. (2018) estimated a 35-91% decrease in global mean cloud albedo forcing over the industrial era when using revised PI fire emission inventories.

70 Emissions of biogenic VOCs (BVOCs), such as isoprene and monoterpenes, from vegetation also affect tropospheric O<sub>3</sub>  
formation. Isoprene contributes to the formation of peroxyacetylnitrate (PAN), which has a lifetime of several months in the  
upper troposphere (Singh, 1987), allowing long-range transport of reactive nitrogen and enhancing O<sub>3</sub> formation in remote  
regions. PAN formation is also highly dependent on NO<sub>x</sub> concentrations, meaning that changes in distribution of emissions as  
well as the magnitude will impact O<sub>3</sub> formation. Previous studies of PI tropospheric O<sub>3</sub> have often assumed that PI BVOC  
75 emissions were equivalent or lower than those in PD (Stevenson et al., 2013). In Stevenson et al. (2013), only one model of  
the ensemble included PI isoprene emissions that were larger than in the PD simulation. However, BVOC emissions are  
sensitive to climate, CO<sub>2</sub> concentrations, vegetation type, and foliage density; each of which has changed since the PI (Hanson  
et al., 2017; Laothawornkitkul et al., 2009) and needs to be accounted for when calculating O<sub>3</sub> RF.

80 Here our aim is to examine the effect of revised PI fire and BVOC emission inventories on PI-PD tropospheric O<sub>3</sub> RF estimates.  
We use a global chemical transport model (CTM) and a radiative transfer model to investigate the impact of these improved  
natural PI emission inventories on PI tropospheric O<sub>3</sub> and how changes in concentration subsequently alter O<sub>3</sub> PI-PD RF. The  
IPCC 5<sup>th</sup> assessment report moved to the concept of effective radiative forcing (ERF) (Myhre et al., 2013) to more completely  
capture the expected global energy budget change from a given driver. However, here we employ the more traditional  
85 stratospherically adjusted RF as it can be estimated with more certainty than ERF and previous studies suggest that ERF and  
RF are likely to be similar for O<sub>3</sub> change (Myhre et al., 2013; Shindell et al., 2013). A number of factors not considered here  
also introduce uncertainty when simulating PI tropospheric O<sub>3</sub> concentrations, such as changes to lightning and soil NO<sub>x</sub>  
emissions, O<sub>3</sub> deposition and atmospheric transport. The purpose of this study is to quantify the uncertainty associated with  
natural emissions in the pre-industrial, utilising the revised inventories of fire and biogenic emissions.

## 90 2 Methods

### 2.1 TOMCAT-GLOMAP

We used the TOMCAT global three-dimensional offline chemical transport model (CTM) (Chipperfield, 2006) coupled to the  
GLOMAP modal aerosol microphysics scheme (Mann et al., 2010) to simulate tropospheric composition and its response to  
emissions changes. The model used a 2.8°×2.8° horizontal resolution with 31 vertical levels from the surface to 10 hPa. All  
95 simulations were run with 6-hourly 2008 meteorology from European Centre for Medium-Range Weather Forecasts (ECMWF)  
ERA-Interim reanalyses with a 1-year spin-up (Dee et al., 2011). The model includes a detailed representation of hydrocarbon  
chemistry and isoprene oxidation, and has previously been shown to accurately reproduce observed concentrations and



distributions of key tropospheric species such as O<sub>3</sub>, CO, NO<sub>x</sub> and VOCs (Monks et al., 2017; Rowlinson et al., 2019). Biomass burning and biogenic emissions are emitted into the lowest model level.

## 100 2.2 Radiative transfer model

Tropospheric O<sub>3</sub> RFs were calculated using the SOCRATES radiative transfer model (Edwards and Slingo, 1996) with six bands in the shortwave (SW) and nine in the longwave (LW). This version has been used extensively in conjunction with TOMCAT-GLOMAP for calculating O<sub>3</sub> radiative effects (Kapadia et al., 2016; Scott et al., 2018; Bekki et al., 2013). We used the fixed dynamical heating approximation (Fels et al., 1980) to account for stratospheric temperature adjustments, i.e. changes in stratospheric heating rate calculated in the model due to the O<sub>3</sub> perturbation are applied to the temperature field, with the model run iteratively until stratospheric temperatures reach equilibrium (Forster and Shine, 1997; Rap et al., 2015).

<i>Simulation</i>	<i>Fire emissions</i>	<i>Biogenic emissions</i>
<i>PD CMIP6</i>	GFEDv4	CCMI
<i>PI CMIP6</i>	CMIP6	CCMI
<i>PI SIMFIRE-BLAZE</i>	SIMFIRE-BLAZE	CCMI
<i>PI LMfire</i>	LMfire	CCMI
<i>PI CMIP6-BIO</i>	CMIP6	LPJ-GUESS
<i>PI SIMFIRE-BLAZE-BIO</i>	SIMFIRE-BLAZE	LPJ-GUESS
<i>PI LMfire-BIO</i>	LMfire	LPJ-GUESS

110 **Table 1. Details of TOMCAT-GLOMAP simulations. All simulations are run with present-day meteorology with a one-year spin-up.**

## 2.3 Simulations

In order to investigate the effect of natural PI emissions on PI to PD changes in tropospheric O<sub>3</sub> concentrations, we performed one PD and six PI TOMCAT simulations. The PD simulation used the Global Fire Emissions Database (GFED) version 4s (GFED v4s) inventory (as employed in CMIP6) (Randerson et al., 2017; van Marle et al., 2017), biogenic emissions from Chemistry-Climate Model Initiative (CCMI) (Sindelarova et al., 2014) and anthropogenic emissions from the MACCity emissions dataset (From EU projects MACC/CityZEN; Lamarque et al., 2010).



Global mean TOMCAT surface CH<sub>4</sub> concentrations are scaled to be 1789 ppb in PD and 722 ppb in the PI (McNorton et al.,  
120 2016; Etheridge et al., 1998; Dlugokencky et al., 2005; Hartmann et al., 2013). In all PI simulations, anthropogenic emissions  
are zero except biofuel emissions taken from AeroCom for the year 1750 (Dentener et al., 2006). The first set of three  
simulations, CMIP6, SIMFIRE-BLAZE and LMfire, investigated the impact of fire emissions only by keeping PI BVOC  
emissions (i.e. isoprene and monoterpenes) at PD values (Table 1). The second set of three simulations, CMIP6-BIO,  
SIMFIRE-BLAZE-BIO and LMfire-BIO, investigated the additional impact of PI biogenic emissions, by combining each PI  
125 fire emission inventory with an estimate of PI BVOC emissions from the LPJ-GUESS model (Table 1).

## 2.4 Fire emission inventories

Following Hamilton et al. (2018), we used three PI inventories to investigate the sensitivity of tropospheric O<sub>3</sub> RF to PI fire  
uncertainty. The CMIP6 PI inventory is treated as a control, as this has been widely used in previous studies and was developed  
130 from a set of global fire models, with SIMFIRE-BLAZE and LMfire providing PI perturbation scenarios from this baseline.

### 2.4.1 CMIP6

CMIP6 provides monthly mean emissions of CO, NO<sub>x</sub>, CH<sub>4</sub> and VOCs from fires. In the PD, CMIP6 emissions are derived  
from satellite estimates of global burden area and active fire detections (Giglio et al., 2013; Randerson et al., 2012). In the  
absence of satellite data, PI CMIP6 fire emissions are generated by merging PD satellite observations with fire proxy records,  
135 visibility records and analysis from six fire models (van Marle et al., 2017). The mean of 1750-1770 emissions is used in this  
study to represent PI emissions. Biomass burning emissions from deforestation and peat fires are assumed to be reduced in the  
PI, while agricultural fires are kept fairly constant with PD due to a lack of information (van Marle et al., 2017).

### 2.4.2 Pre-industrial SIMFIRE-BLAZE

The SIMFIRE-BLAZE PI fire emission inventory was developed using the LPJ-GUESS-SIMFIRE-BLAZE model. The PI  
140 emissions here are the mean for the period 1750-1770 (Hamilton et al., 2018). The LPJ-GUESS dynamic vegetation model  
predicts ecosystem properties for given climate variables (Smith et al., 2014), which, combined with the HYDE 3.1 dataset of  
human land-use change, allows simulation of global PI land cover (Klein Goldewijk et al., 2011). The SIMple fire model  
(SIMFIRE) calculates total burned area (Knorr et al., 2014) with total fire carbon-flux calculated from BLAZE (BLAZE  
induced biosphere-atmosphere flux Estimator) (Rabin et al., 2017). Akagi et al. (2011) emissions factors were used with  
145 separate treatment of herbaceous and non-herbaceous, tropical and extratropical vegetation to produce emission inventories.  
Agricultural fire emissions are not included in SIMFIRE-BLAZE. Total PI fire emissions of gas species in the SIMFIRE-  
BLAZE inventory are 28% larger than in the PI CMIP6 inventory.



### 2.4.3 Pre-industrial LPJ-LMfire

The LPJ-LMfire model calculates dry matter consumed by fire and simulates natural wildfire ignition from lightning (Murray et al., 2014; Pfeiffer et al., 2013). Land use is prescribed for the year 1770 using the KK10 scenario from Kaplan et al. (2011). Akagi et al. (2011) emissions factors were again used to calculate the gas-phase fire emissions from dry biomass burned in each grid cell. Burned area is calculated based on fuel availability. LMfire includes emissions from managed agricultural burning, with 50% of the litter on 20% of used croplands burdened annually. Also included are emissions from post-harvest agricultural burning, with 10% of harvested agricultural crop material assumed to be burned each year. Total PI fire emissions in LMfire are approximately double the SIMFIRE-BLAZE inventory and four times larger than CMIP6 emissions.

### 2.5 Assessment of PI fire emissions

Despite being significantly larger than CMIP6 and SIMFIRE-BLAZE (Fig. 1), emissions from LMfire have been shown to be within the quantifiable uncertainty of fire emissions (Lee et al., 2013). Furthermore, LMfire compares more favourably than the CMIP6 and SIMFIRE-BLAZE inventories with Northern Hemisphere (NH) ice core records in Greenland and Wyoming (Chellman et al., 2017; Hamilton et al., 2018). In addition to the examination of paleoenvironmental archives with PI fire emissions datasets by Hamilton et al. (2018), we compared simulated annual mean surface PI CO concentrations in Antarctica for each fire emissions inventory using the Southern Hemisphere (SH) ice core CO record from Wang et al. (2010). Simulated Antarctic CO concentrations using PI CMIP6 emissions are 37 ppb, substantially lower than the Wang et al. (2010) 1750 value of  $45 \pm 5$  ppb. This CMIP6 value is closer to the 650-year minimum that occurred in the mid-17<sup>th</sup> century (38 ppb). When using SIMFIRE-BLAZE and LMfire emissions, Antarctic CO concentrations for 1750 are estimated at 48 ppb and 61 ppb, respectively. The overestimation when using LMfire suggest that SH CO emissions may be high for 1750; however, they are comparable to the peak CO concentration measured in the late 1800s ( $55 \pm 5$  ppb) when fire emissions also peaked (van der Werf et al., 2013). As 1850 is also sometimes used as the PI baseline year when calculating RF, we suggest LMfire provides a realistic upper bound to possible PI fire emissions.

170

The combined evaluation of these inventories in Hamilton et al. (2018) and here indicates that although the revised PI fire inventories differ considerably from each other and are larger than CMIP6, they are closer to proxy records than CMIP6 estimates and therefore their respective impacts on tropospheric O<sub>3</sub> RF need to be considered.

### 2.6 Biogenic emission inventories

#### 2.6.1 Present-day CCMi

The PD control biogenic emissions were provided from the CCMi inventory. CCMi mean annual BVOC emissions, comprising isoprene and monoterpenes, are derived using the Model of Emissions of Gases and Aerosols from Nature (MEGAN) model (Guenther et al., 2012) under the MACC project (Sindelarova et al., 2014). The CCMi inventory estimates



global BVOC emissions at 623 Tg/yr, in reasonable agreement with surface flux measurements and other modelling studies  
180 (Sindelarova et al., 2014; Arneth et al., 2008; Rap et al., 2018).

## 2.6.2 LPJ-GUESS

Alternative biogenic emissions were produced using the LPJ-GUESS dynamic vegetation model simulating isoprene and  
monoterpenes (Arneth et al., 2007; Schurgers et al., 2009). Total PD emissions and distribution in the LPJ-GUESS inventory  
(i.e. 607 Tg/yr) are similar to the PD CCMI inventory (Fig. 2). For the PI emissions, the LPJ-GUESS biogenic emissions  
185 inventory is based on the mean for the period 1750-1770, estimated to be 836 Tg/yr. There are large spatial differences between  
the PI LPJ-GUESS and PD CCMI inventories, with significantly higher emissions in South America and Central Africa, and  
lower emissions in South-East Asia in the PI LPJ-GUESS inventory (Fig. 2).

## 3 Results and discussion

### 3.1 Pre-industrial emission inventories

190 Figure 1a-d shows annual latitudinal fire emissions of CO, NO<sub>x</sub>, CH<sub>4</sub> and VOCs for the CMIP6, SIMFIRE-BLAZE and LMfire  
PI inventories, compared to the PD CMIP6 inventory. We also compare BVOC emissions (i.e. isoprene and all monoterpenes)  
from the LPJ-GUESS inventory with the PD CCMI inventory. In the PI CMIP6 simulation, global CO emissions have  
increased by a factor of 2.5 between PI and PD from 381 Tg/yr to 970 Tg/yr. The main driver of this increase is industrial  
emissions, particularly in the NH mid-latitudes. There is large variation in simulated CO emissions between the three PI fire  
195 inventories: 644 Tg/yr in SIMFIRE-BLAZE (69% larger than CMIP6) and 1152 Tg/yr in LMfire (200% larger). Estimates of  
CO emissions using LMfire results in total global emissions which are larger than the PD estimate, which also includes  
anthropogenic sources. The larger PI biomass burning emissions in LMfire are a result of a number of factors not present in  
the other PI inventories such as the inclusion of high-latitude fire occurrence, agricultural fire emissions and differing emission  
factors (Hamilton et al., 2018).

200

Global NO<sub>x</sub> emissions also vary considerably between PI inventories, with values in the SIMFIRE-BLAZE inventory  
increasing 13% compared to the CMIP6 inventory (36 Tg/yr compared to 32 Tg/yr). This difference is largely due to increased  
emission in NH mid-latitudes within SIMFIRE-BLAZE. NO<sub>x</sub> emissions in LMfire are 112% larger than the CMIP6 total (68  
Tg/yr), with the most significant increases in the extra-tropics.

205

As CH<sub>4</sub> emissions from fires are significantly smaller than CO emissions (Voulgarakis and Field, 2015) increased PI fire  
estimates do not substantially alter total CH<sub>4</sub> emission. CH<sub>4</sub> emissions in SIMFIRE-BLAZE and LMfire are similar in amount  
and distribution, 15% and 9% lower than CMIP6, respectively. There is an increase in SH CH<sub>4</sub> emissions in both SIMFIRE-  
BLAZE and LMfire compared to CMIP6 but a decrease in the NH and SH mid-latitudes. Total PI CH<sub>4</sub> emissions are greatest



210 in CMIP6 at 241 Tg/yr, approximately 43% of PD emissions. Due to the scaling of global mean surface CH<sub>4</sub> concentrations  
in TOMCAT-GLOMAP, the effect of changes in amount of CH<sub>4</sub> emitted will be very small, however the change in distribution  
may impact the formation and loss rates of tropospheric O<sub>3</sub>.

In terms of fire-emitted VOC species, their size and distribution of emissions are fairly consistent between PD and PI  
215 inventories. PI CMIP6 are 87% of PD CMIP6 values, with PI SIMFIRE-BLAZE at 97% (303 Tg/yr). Total global VOC  
emissions are largest in LMfire at 349 Tg/yr, 29% larger than PI CMIP6 (271 Tg/yr) and 13% larger than PD CMIP6 (310  
Tg/yr). The distribution of global VOC emissions is relatively uniform across all inventories, however, individual species do  
have larger variability between inventories. Formaldehyde and acetylene for example have substantially increased SH  
emissions in SIMFIRE-BLAZE and LMfire.

220

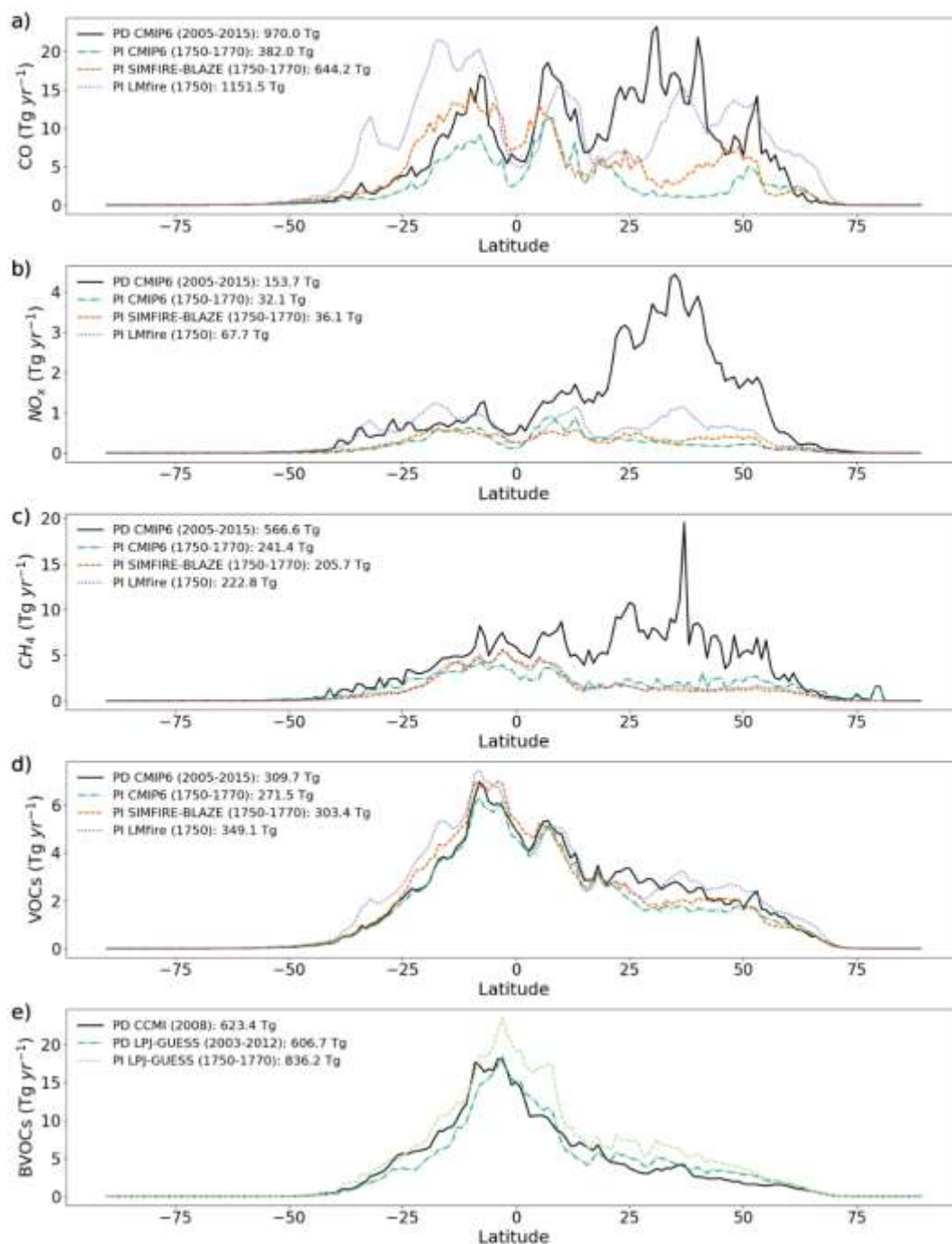


**Figure 1: Annual latitudinal mean fire emissions (in Tg/yr) of (a) CO, (b) NO<sub>x</sub>, (c) CH<sub>4</sub> and (d) VOCs and annual zonal mean BVOC emissions (e), for PD (solid black line), PI CMIP6 (dashed green), PI SIMFIRE-BLAZE (dotted orange), PI LMfire (dashed purple), PD LPJ-GUESS (dashed dark green) and PI LPJ-GUESS (dotted light green).**



225

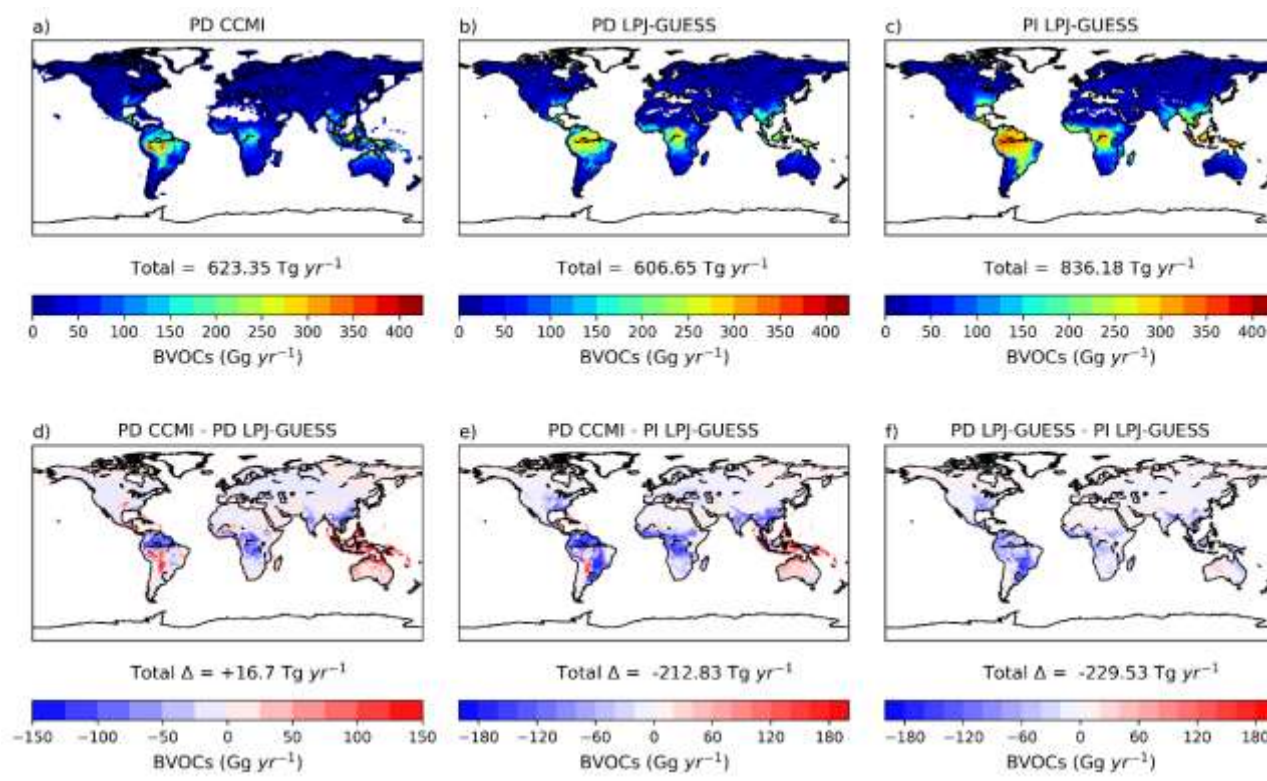
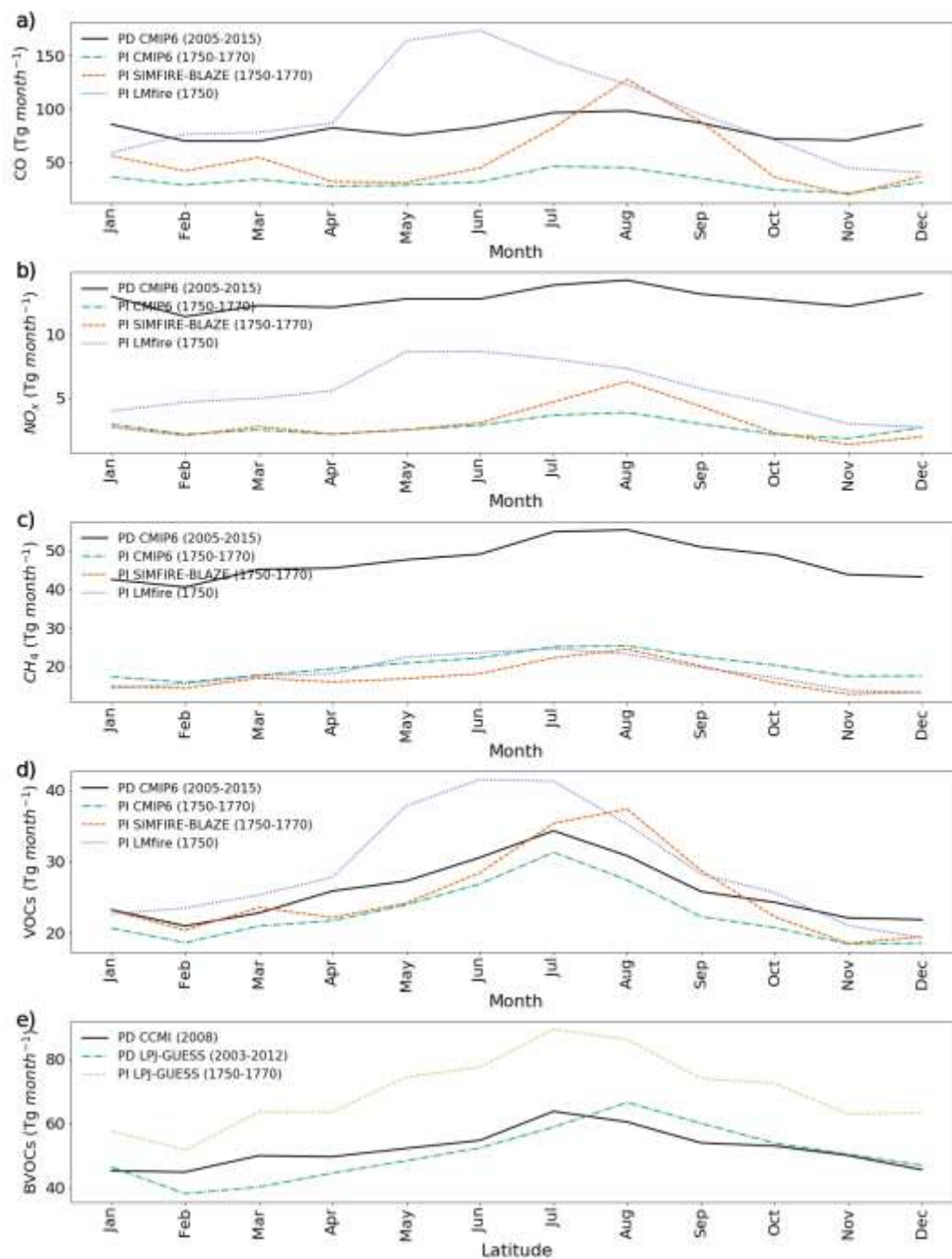


**Figure 2: Annual BVOC (isoprene + monoterpenes) emissions in the two present-day biogenic emissions inventories (CCMI and LPJ-GUESS) and the preindustrial LPJ-GUESS inventory. Top panels (a-c) show total emissions per year, while lower panels (d-f) show differences between the three inventories. Total annual emissions and difference in annual emissions are also shown.**

230

The BVOC emissions in the two PD inventories (CCMI and LPJ-GUESS) are similar (Fig. 1e), although a small positive NH gradient exists in PD LPJ-GUESS compared to PD CCMI. Total BVOC emissions are 16.7 Tg larger in the PD CCMI inventory than PD LPJ-GUESS (Fig. 2). However, the PI LPJ-GUESS BVOC estimate (836 Tg/yr) is 37% larger than its PD equivalent and 34% larger than PD CCMI, although with a similar spatial distribution (Fig. 2). The largest difference is in South American emissions, where PI LPJ-GUESS emissions are up to 120 Tg larger than PD. The reduction of BVOC emissions between PI and PD is due to a combination of crop expansion, land cover changes and CO<sub>2</sub> inhibition (Hantson et al., 2017). Our results are consistent with previous studies reporting between ~25% (Pacifico et al., 2012; Hollaway et al., 2017; Lathièrè et al., 2010) and ~35% (Unger, 2014) larger PI values than PD.

235

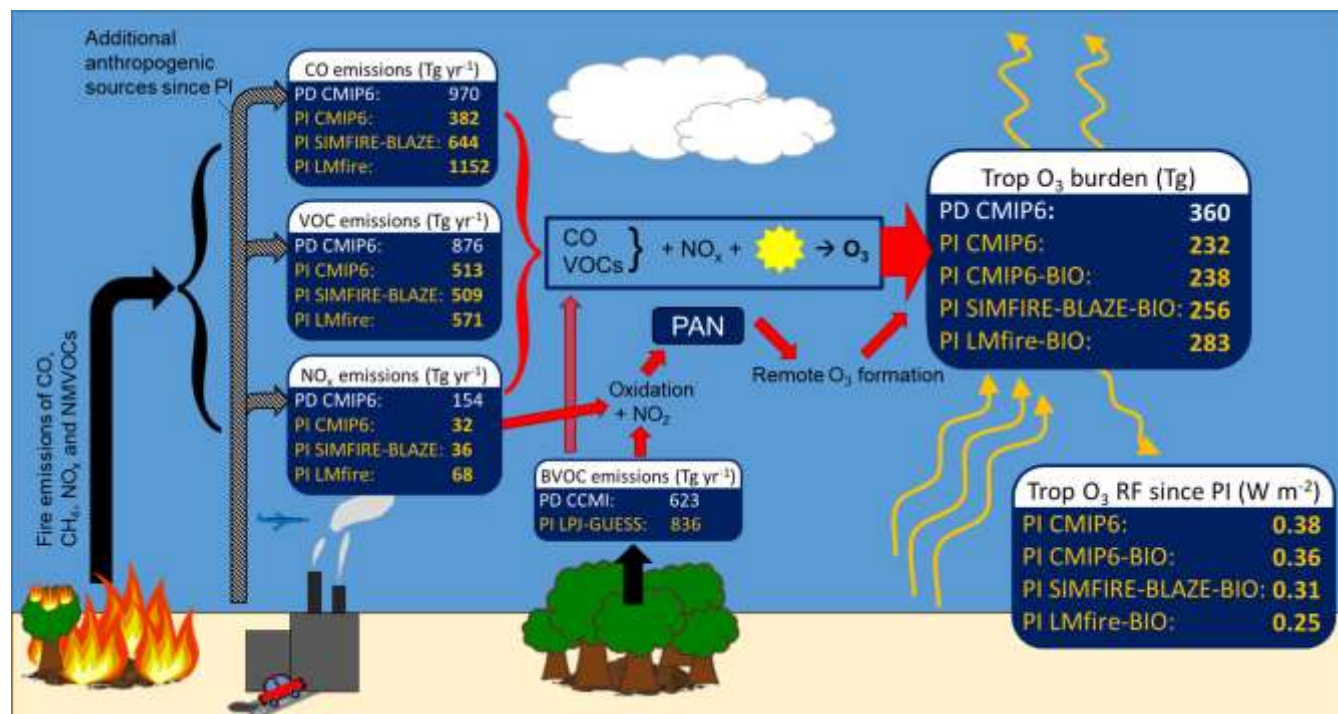


240 **Figure 3: Total monthly fire emissions (in Tg/month) of (a) CO, (b) NO<sub>x</sub>, (c) CH<sub>4</sub> and (d) VOCs and total monthly BVOC emissions (e), for PD (solid black line), PI CMIP6 (dashed green), PI SIMFIRE-BLAZE (dotted orange), PI LMfire (dashed purple), PD LPJ-GUESS (dashed dark green) and PI LPJ-GUESS (dotted light green).**



The seasonality of the fire emissions in the PD and PI inventories used here is demonstrated in Fig. 3. CMIP6 PI and PD emissions have an extremely similar seasonal cycle for all species, with maximum emissions of precursors between July and September. This is expected as the PI CMIP6 emissions are based on GFED4s climatology and monthly patterns were assumed not to have changed over time (van Marle et al., 2017). This also reflects the PD seasonal cycle of tropospheric O<sub>3</sub> in the SH, where anthropogenic contributions are lower than the NH, with maximum concentrations found in September/October (Cooper et al., 2014). The seasonal cycle of CO emissions (Fig. 3a) varies substantially across the 3 PI inventories, with LMfire estimating peak emissions in May-June as opposed to July-August in CMIP6 and SIMFIRE-BLAZE. This may be a result of increased emissions from SH Africa and Central America, where large fire events are common in late-spring. The inclusion of high-latitude fire occurrence and agricultural burning in LMfire may also play a role, as these contribute to fire emissions in the boreal spring season (Hamilton et al., 2018). The SIMFIRE-BLAZE CO emissions exhibit a similar but more pronounced seasonal cycle to that in CMIP6, with peak emissions in August. Similarly, NO<sub>x</sub> and VOC emissions peak earlier in the year in the LMfire inventory relative to SIMFIRE-BLAZE and CMIP6, again with a larger peak in August in SIMFIRE-BLAZE. Monthly CH<sub>4</sub> emissions are broadly consistent across all inventories, with peak emissions in July or August and lower emissions over the NH winter. The seasonality of BVOCs emissions is also consistent across all PI inventories and PD CMIP6, with a peak in July-August. Isoprene emissions are heavily dependent on temperature and photosynthetic active radiation (Malik et al., 2018), therefore reach a maximum in NH summer when these parameters are at optimum for vegetation emissions.

Figure 3 indicates similar controls over the modelled seasonality of PI fire occurrence in both PI CMIP6 and PI SIMFIRE-BLAZE, although an increase in estimated fire extent in SIMFIRE-BLAZE resulting in a more pronounced seasonal cycle. LMfire on the other hand estimates a shift in the seasonality of global fire emissions, with peak fire emission occurring earlier than other inventories, as well as a broader peak period of emissions. The change in seasonality of precursors will affect the formation and transport of simulated tropospheric O<sub>3</sub> concentrations, as atmospheric chemistry and circulation also have strong seasonal cycles. However, the broadly similar pattern of maximum emissions in the NH summer and a minimum in NH winter, coinciding with similar climatic conditions, means that the substantial difference in volume of precursor emissions across the PI inventories is likely to be more significant than seasonal changes.



270 **Figure 4: Summary schematic showing tropospheric O<sub>3</sub> precursor emissions from fire, biogenic and anthropogenic sources, the processes of photochemical O<sub>3</sub> formation, the tropospheric O<sub>3</sub> burden and the PI-PD RF. The magnitude of CO, NO<sub>x</sub>, VOC and BVOC precursor emissions used in this study is shown for the PD (white text) and each PI inventory (yellow text). The resulting calculated tropospheric O<sub>3</sub> burden and RF when using each emission inventory are also shown.**

### 3.2 Pre-industrial fire emissions effect on O<sub>3</sub>

275 Annual emissions of O<sub>3</sub> precursors, their simulated annual mean PI burdens and their contribution to the formation of tropospheric O<sub>3</sub> are shown in Fig. 4 and Table 2. The largest difference between simulations is in the simulated global tropospheric CO burden which varies by up to 100 Tg depending on the PI fire emission inventory employed: 195 Tg in the PI CMIP6 simulation, 232 Tg in PI SIMFIRE-BLAZE (18% higher than CMIP6) and 295 Tg in PI LMfire (50% higher) (Table 2).

280 The difference in global NO<sub>x</sub> burden between PI simulations is smaller, with increases of 4% and 18% in PI SIMFIRE-BLAZE and PI LMfire respectively, relative to PI CMIP6. The annual mean NH/SH ratio of tropospheric NO<sub>x</sub> burden in PI simulations is 1.09, 1.12 and 1.18 for CMIP6, SIMFIRE-BLAZE and LMfire, respectively. Simulated airmass-weighted global mean concentrations of tropospheric OH, which plays a key role in tropospheric O<sub>3</sub> formation, are 1.06, 1.06 and 1.11 × 10<sup>6</sup> molecules cm<sup>-3</sup> in CMIP6, SIMFIRE-BLAZE and LMfire, respectively. These values all fall within one standard deviation of the  
 285 Atmospheric Chemistry and Climate Model Intercomparison Project (ACCMIP) multi-model mean of 1.13 ± 0.17 (Naik et al., 2013). PI OH concentrations are lower than PD simulated values (1.12 × 10<sup>6</sup> molecules cm<sup>-3</sup>), due to the higher concentrations of OH precursors NO<sub>x</sub> and O<sub>3</sub> in PD outcompeting the effect of increased CH<sub>4</sub> and CO concentrations which deplete OH (Naik



et al., 2013). The NH/SH OH ratio is  $1.25 \pm 0.02$  in the PI simulations compared to 1.41 in the PD CMIP6 simulation, slightly larger than the corresponding ACCMIP multi-model mean values ( $1.13 \pm 0.09$  and  $1.28 \pm 0.10$ , respectively) but within the inter-  
290 model range and reflecting the expected PI to PD increase (Naik et al., 2013).

Changes to the atmospheric concentration and distribution of  $O_3$  precursor species lead to changes in the tropospheric  $O_3$  burden. The PI CMIP6 simulation produced the lowest tropospheric  $O_3$  burden at 232 Tg, slightly below the ACCMIP multi-model mean of 239 Tg for 1850 (Young et al., 2013). In PI SIMFIRE-BLAZE the burden is 242 Tg (4% higher than CMIP6)  
295 while in LMfire it is 273 Tg (18% higher), slightly outside the range of estimates of 1850 tropospheric  $O_3$  burden in ACCMIP models (192 Tg to 272 Tg) (Young et al., 2013). The burdens simulated here represent a PI to PD tropospheric  $O_3$  burden change of 55%, 49% and 32% for CMIP6, SIMFIRE-BLAZE and LMfire, respectively. We note that in these simulations the PI LMfire is the only inventory leading to a simulated PI to PD global burden change of less than 40%, a value consistent with that recently indicated by isotope measurements in ice cores (Yeung et al., 2019). The differences between CMIP6 and  
300 SIMFIRE-BLAZE are primarily related to increases in tropospheric  $O_3$  within the Amazon region (Fig. 5a). The change in tropospheric  $O_3$  vertical profile in the PI SIMFIRE-BLAZE simulation compared to PI CMIP6 (Fig. 5c) shows increased annual mean concentrations throughout the troposphere, driven by changes at 30°S and 50°N. Changes between LMfire and CMIP6 simulated tropospheric  $O_3$  profiles are larger, with increased  $O_3$  at all latitudes. Compared to PI CMIP6, there is a mean global increase in  $O_3$  column of 3.7 DU when using LMfire and 1.0 DU when using SIMFIRE-BLAZE. The largest changes  
305 occur over Central Asia, Australia and South America where tropospheric column  $O_3$  can be as much as 9.0 DU higher in the PI LMfire simulation than the PI CMIP6 simulation (Fig. 5b). This is reflected in the changes to the vertical  $O_3$  profile, with the largest increases in the subtropics. The difference between LMfire and CMIP6 simulations is greatest between 600 and 800 hPa in the SH, and is roughly constant with respect to changes in altitude over the northern subtropics. The only regions where tropospheric  $O_3$  is higher in the CMIP6 simulation are Central Africa and Indonesia, likely due to the PI CMIP6  
310 emissions being anchored to PD fire observations and thus transferring these patterns to the PI (van Marle et al., 2017).

The effect of different fire emission inventories on  $O_3$  burden is significantly smaller than the impact on CO concentrations (Table 2), as fire emissions are one of several sources of  $O_3$  variability (Lelieveld and Dentener, 2000).  $O_3$  production is reliant on a number of precursors which do not respond uniformly to the different estimates of fire occurrence in the inventories used  
315 here. The relatively minor response of  $NO_x$  concentrations across the three PI emissions estimates (Table 2), and the prevailing  $NO_x$ -limited state across rural environments in PD (Duncan et al., 2010), suggests that increases in CO and VOCs have only a small impact on  $O_3$  production because of  $NO_x$  availability limitations. Moreover, Stevenson et al. (2013) attributed the majority of the PI to PD shift in tropospheric  $O_3$  to  $NO_x$  and  $CH_4$  changes, with a relatively small contribution from CO and NMVOCs despite increasing emissions of both. However, the simulated changes still represent significant shifts in the  
320 abundance and distribution of tropospheric  $O_3$  in the PI atmosphere.



	CO burden (Tg)	NO <sub>x</sub> burden (Tg)	Mean tropospheric OH (x10 <sup>6</sup> mol cm <sup>-3</sup> )	O <sub>3</sub> burden (Tg)	Tropospheric column O <sub>3</sub> (DU)	O <sub>3</sub> RF 1750-2010 (Wm <sup>-2</sup> )
<b>PD CMIP6</b>	342.6	73.2	1.12	359.9	31.0	-
<b>PI CMIP6</b>	195.5	44.8	1.06	231.7	19.9	0.38
<b>PI SIMFIRE-BLAZE</b>	231.5	46.7	1.06	241.6	20.9	0.35
<b>PI LMfire</b>	295.0	52.8	1.11	272.7	23.6	0.27
<b>PI CMIP6-BIO</b>	238.7	44.3	1.00	237.8	20.2	0.36
<b>PI SIMFIRE-BLAZE-BIO</b>	283.4	46.7	1.00	256.0	22.1	0.31
<b>PI LMfire-BIO</b>	337.1	53.4	1.08	282.8	24.4	0.25

Table 2: Annual mean global tropospheric burdens of CO, NO<sub>x</sub> and O<sub>3</sub>, mean tropospheric OH concentration, tropospheric column O<sub>3</sub> in Dobson units (DU) and radiative forcing of tropospheric O<sub>3</sub> 1750-2010 for present-day simulation and each PI fire and biogenic emission inventory.

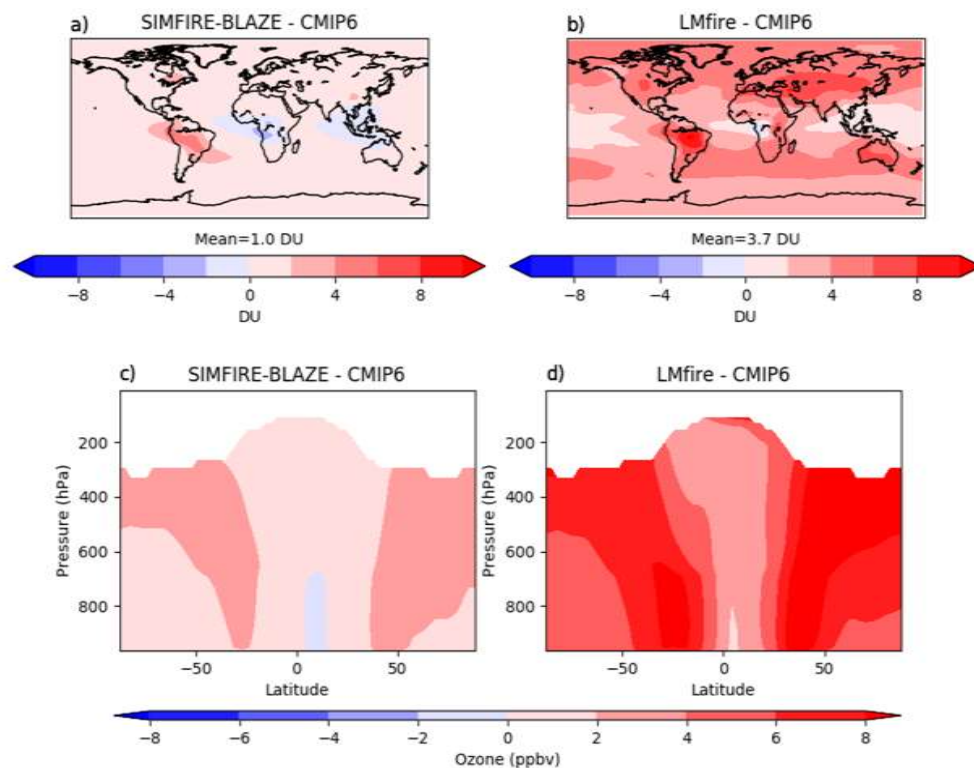


**Figure 5: Difference in simulated PI O<sub>3</sub> between revised inventories SIMFIRE-BLAZE and LMfire and the CMIP6 control. Top panels (a, b) compare differences in tropospheric column O<sub>3</sub> in DU, lower panels (c, d) show differences in zonal mean vertical O<sub>3</sub> in ppbv.**

### 3.3 Pre-industrial BVOC emissions effect on O<sub>3</sub>

We repeated the three PI simulations, replacing the PD biogenic emissions with the PI LPJ-GUESS inventory. In general, the inclusion of PI BVOC emissions increases PI O<sub>3</sub> concentrations, due to an increased VOC source and hence PAN formation (Fig. 4). For CMIP6 fire emissions, the inclusion of PI BVOCs increases the CO burden by 22% and tropospheric O<sub>3</sub> burden by 3%, while mean tropospheric OH concentration decreases by 6%. The decrease in OH is the most likely reason for the simulated increases in CO and O<sub>3</sub>. The inclusion of PI BVOCs in the LMfire fire emission simulation causes a 3% decrease in tropospheric OH, and increases in tropospheric CO and O<sub>3</sub> of 14% and 4%, respectively.

330

For SIMFIRE-BLAZE, the inclusion of PI BVOCs decreases OH by 6% and increases CO and O<sub>3</sub> by 22% and 6%, respectively. In all simulations the inclusion of PI BVOCs has only a small effect on the NO<sub>x</sub> burden (~1%). The effect on tropospheric O<sub>3</sub> of including PI BVOCs is notably larger in the simulation using SIMFIRE-BLAZE fire emissions compared to CMIP6 or LMfire. The SIMFIRE-BLAZE simulation combines fire and biogenic emissions produced using the same land-use model, with consistent vegetation distributions. The co-location of isoprene and NO<sub>x</sub> emissions promotes PAN formation, enabling long-range transport of NO<sub>x</sub> and enhancing O<sub>3</sub> production (Hollaway et al., 2017). This synergistic effect has been found to amplify the effect of biogenic emissions on tropospheric O<sub>3</sub> production (Bossioli et al., 2012). Therefore, if PI biogenic emissions inventories were specifically produced for each fire inventory, the corresponding impact on O<sub>3</sub> would likely be larger than presented here. With the inclusion of PI BVOC emissions, both the SIMFIRE-BLAZE and LMfire simulations

335



340 result in a PI to PD tropospheric O<sub>3</sub> burden change of 40% or less, in line with estimates from ice core observations (Yeung et al., 2019).

### 3.4 Effect on ozone radiative forcing

The estimated tropospheric O<sub>3</sub> RF, based on the CMIP6 PI and PD control simulations, is 0.38 Wm<sup>-2</sup> (Fig. 4 and Table 2), comparing well with the IPCC AR5 estimate of 0.4 ± 0.2 Wm<sup>-2</sup> (Myhre et al., 2013) and the ACCMIP multi-model mean of  
345 0.41 ± 0.12 Wm<sup>-2</sup> (Stevenson et al., 2013; Myhre et al., 2013). When PI SIMFIRE-BLAZE and PI LMfire emissions are used instead of PI CMIP6 fire emissions, larger PI tropospheric O<sub>3</sub> concentrations lead to 8% (to 0.35 Wm<sup>-2</sup>) and 29% (to 0.27 Wm<sup>-2</sup>) decreases in O<sub>3</sub> RF, respectively. When the PI BVOC emission inventory is used in conjunction with each PI fires emission inventory, O<sub>3</sub> RF is further reduced compared to the control by 5% (to 0.36 Wm<sup>-2</sup>), 18% (to 0.31 Wm<sup>-2</sup>) and 34% (to 0.25 Wm<sup>-2</sup>), for CMIP6, SIMFIRE-BLAZE and LMfire, respectively (Fig. 4). While these reductions in O<sub>3</sub> RF are still within the IPCC  
350 uncertainty range, they are caused entirely by uncertainty in PI precursor emissions from wildfires and vegetation. Other key sources of uncertainty (e.g. inter-model spread, use of different radiative transfer schemes) are not accounted for here and would therefore alter estimates further, potentially outside the current 5%-95% confidence range. The most important region for changes to the RF of O<sub>3</sub> is the upper troposphere at subtropical latitudes (Fig. 5d), where there are substantially higher O<sub>3</sub> concentrations in the LMfire simulation. O<sub>3</sub> changes in this region are up to 10 times more efficient at altering the radiative  
355 flux than in other regions (Rap et al., 2015). However, the lack of a vertical distribution to fire emissions in TOMCAT affects the simulated changes to the O<sub>3</sub> vertical profile. Previous studies which introduced an injection height scheme found small increases in O<sub>3</sub> production downwind of emission sources (Jian and Fu, 2014), although the change to total O<sub>3</sub> and precursors is relatively small (Bossioli et al., 2012; Zhu et al., 2018).

## 4 Conclusions

360 Revised inventories of PI fire and biogenic emissions substantially decrease estimates of PI to PD tropospheric O<sub>3</sub> RF. When using PI LMfire fire emissions, which represent a plausible upper emissions limit, O<sub>3</sub> RF is reduced to 0.27 Wm<sup>-2</sup>, 29% smaller than the CMIP6 simulation. Large increases in estimated PI fire occurrence drives increases in PI O<sub>3</sub> concentrations (3.7 DU global mean tropospheric column O<sub>3</sub> increase for LMfire inventory) through larger emissions of CO, NO<sub>x</sub> and VOCs. PI CO increases by up to 51% depending on the PI inventory, but the effect on O<sub>3</sub> production is limited by the relatively small increase  
365 in NO<sub>x</sub> (~4%). Using PI biogenic emissions, rather than assuming PD values, further increases simulated PI tropospheric O<sub>3</sub>, though the magnitude of this depends on the fire inventory. When accounting for revised emissions from fire and biogenic sources, both the LMfire and SIMFIRE-BLAZE inventories simulated a PI to PD change in tropospheric O<sub>3</sub> burden of approximately 40% or less, in good agreement with estimates from Yeung et al. (2019). Consequently, we find that the estimate of O<sub>3</sub> RF since PI decreases by up to 34% (to 0.25 Wm<sup>-2</sup>) when considering the uncertainty in PI emissions of both fires and  
370 BVOCs.

The impact on tropospheric O<sub>3</sub> from uncertainty in PI natural emissions suggests that previous estimates of O<sub>3</sub> RF over the industrial era are likely too large. Our revised tropospheric O<sub>3</sub> RF estimates are at the lower end of the existing uncertainty range, without yet taking into account other sources of uncertainty. We therefore argue that the impact of uncertainty in PI  
375 natural emissions should be further investigated using more models, in order to reassess the current best-estimate and uncertainty range of O<sub>3</sub> RF.



### Acknowledgements

MJR is funded by a NERC SPHERES DTP (NE/L002574/1) studentship. This work used the UK ARCHER (<http://www.archer.ac.uk>) and Leeds ARC3 high performance computing facilities. RP is funded by the UK National Centre for Earth Observation (NCEO). SH and AA acknowledge support from EU FP7 projects BACCHUS (grant agreement No. 603445) and LUC4C (grant agreement No. 603542). DSH is funded by the Atkinson Center for a Sustainable Future at Cornell University. PF supported by NERC grant NE/N006038/1 (SMURPHS) and EU Horizon 2020 program grant agreement number 820829 (CONSTRAIN). Datasets available via Open Science Framework (<https://osf.io/98c2n/>).

### Author contribution

385 MJR, AR, DSH and RJP conceptualised the study and planned the model experiments. Emission inventories were produced by SH, JOK, AA and LN, and processed for use in TOMCAT-GLOMAP by RJP and DSH. All model runs and analysis was performed by MJR with guidance from AR, RJP and SRA. The manuscript was written by MJR with comments and advice from all co-authors.

390



## References

- Akagi, S. K., Yokelson, R. J., Wiedinmyer, C., Alvarado, M. J., Reid, J. S., Karl, T., Crounse, J. D., and Wennberg, P. O.: Emission factors for open and domestic biomass burning for use in atmospheric models, *Atmos. Chem. Phys.*, 11, 4039-4072, 10.5194/acp-11-4039-2011, 2011.
- 395 Andela, N., Morton, D. C., Giglio, L., Chen, Y., van der Werf, G. R., Kasibhatla, P. S., DeFries, R. S., Collatz, G. J., Hantson, S., Kloster, S., Bachelet, D., Forrest, M., Lasslop, G., Li, F., Mangeon, S., Melton, J. R., Yue, C., and Randerson, J. T.: A human-driven decline in global burned area, 356, 1356-1362, 10.1126/science.aal4108 %J Science, 2017.
- Arneth, A., Niinemets, Ü., Pressley, S., Bäck, J., Hari, P., Karl, T., Noe, S., Prentice, I. C., Serça, D., Hickler, T., Wolf, A., and Smith, B.: Process-based estimates of terrestrial ecosystem isoprene emissions: incorporating the effects of a direct CO<sub>2</sub>-isoprene interaction, *Atmos. Chem. Phys.*, 7, 31-53, 10.5194/acp-7-31-2007, 2007.
- 400 Arneth, A., Monson, R. K., Schurgers, G., Niinemets, Ü., and Palmer, P. I.: Why are estimates of global terrestrial isoprene emissions so similar (and why is this not so for monoterpenes)?, *Atmos. Chem. Phys.*, 8, 4605-4620, 10.5194/acp-8-4605-2008, 2008.
- Arneth, A., Sitch, S., Bondeau, A., Butterbach-Bahl, K., Foster, P., Gedney, N., de Noblet-Ducoudré, N., Prentice, I. C., Sanderson, M., Thonicke, K., Wania, R., and Zaehle, S.: From biota to chemistry and climate: towards a comprehensive description of trace gas exchange between the biosphere and atmosphere, *Biogeosciences*, 7, 121-149, 10.5194/bg-7-121-2010, 2010.
- Bekki, S., Rap, A., Poulain, V., Dhomse, S., Marchand, M., Lefevre, F., Forster, P. M., Szopa, S., and Chipperfield, M. P.: Climate impact of stratospheric ozone recovery, 40, 2796-2800, 10.1002/grl.50358, 2013.
- 410 Bossioli, E., Tombrou, M., Karali, A., Dandou, A., Paronis, D., and Sofiev, M.: Ozone production from the interaction of wildfire and biogenic emissions: a case study in Russia during spring 2006, *Atmos. Chem. Phys.*, 12, 7931-7953, 10.5194/acp-12-7931-2012, 2012.
- Bowman, D. M. J. S., Balch, J. K., Artaxo, P., Bond, W. J., Carlson, J. M., Cochrane, M. A., D'Antonio, C. M., DeFries, R. S., Doyle, J. C., Harrison, S. P., Johnston, F. H., Keeley, J. E., Krawchuk, M. A., Kull, C. A., Marston, J. B., Moritz, M. A., Prentice, I. C., Roos, C. I., Scott, A. C., Swetnam, T. W., van der Werf, G. R., and Pyne, S. J.: Fire in the Earth System, *Science*, 324, 481-484, 10.1126/science.1163886, 2009.
- 415 Checa-Garcia, R., Hegglin, M. I., Kinnison, D., Plummer, D. A., and Shine, K. P.: Historical Tropospheric and Stratospheric Ozone Radiative Forcing Using the CMIP6 Database, *Geophysical Research Letters*, 45, 3264-3273, 10.1002/2017GL076770, 2018.
- 420 Chellman, N., McConnell, J. R., Arienzo, M., Pederson, G. T., Aarons, S. M., and Csank, A.: Reassessment of the Upper Fremont Glacier Ice-Core Chronologies by Synchronizing of Ice-Core-Water Isotopes to a Nearby Tree-Ring Chronology, *Environmental Science & Technology*, 51, 4230-4238, 10.1021/acs.est.6b06574, 2017.
- Chipperfield, M. P.: New version of the TOMCAT/SLIMCAT off-line chemical transport model: Intercomparison of stratospheric tracer experiments, *Quarterly Journal of the Royal Meteorological Society*, 132, 1179-1203, doi:10.1256/qj.05.51, 2006.
- 425 Cooper, O. R., Parrish, D., Ziemke, J., Balashov, N., Cupeiro, M., Galbally, I., Gilge, S., Horowitz, L., R. Jensen, N., Lamarque, J.-F., Naik, V., Oltmans, S., Schwab, J., T. Shindell, D., Thompson, A., Thouret, V., Wang, Y., and Zbinden, R.: Global distribution and trends of tropospheric ozone: An observation-based review, 000029 pp., 2014.
- Daniau, A. L., Bartlein, P. J., Harrison, S. P., Prentice, I. C., Brewer, S., Friedlingstein, P., Harrison-Prentice, T. I., Inoue, J., Izumi, K., Marlon, J. R., Mooney, S., Power, M. J., Stevenson, J., Tinner, W., Andrić, M., Atanassova, J., Behling, H., Black, M., Blarquez, O., Brown, K. J., Carcaillet, C., Colhoun, E. A., Colombaroli, D., Davis, B. A. S., D'Costa, D., Dodson, J., Dupont, L., Eshetu, Z., Gavin, D. G., Genies, A., Haberle, S., Hallett, D. J., Hope, G., Horn, S. P., Kassa, T. G., Katamura, F., Kennedy, L. M., Kershaw, P., Krivonogov, S., Long, C., Magri, D., Marinova, E., McKenzie, G. M., Moreno, P. I., Moss, P., Neumann, F. H., Norström, E., Paitre, C., Rius, D., Roberts, N., Robinson, G. S., Sasaki, N., Scott, L., Takahara, H., Terwilliger, V., Thevenon, F., Turner, R., Valsecchi, V. G., Vannière, B., Walsh, M., Williams, N., and Zhang, Y.: Predictability of biomass burning in response to climate changes, *Global Biogeochemical Cycles*, 26, 10.1029/2011GB004249, 2012.
- 435 Dee, D. P., Uppala, S. M., Simmons, A. J., Berrisford, P., Poli, P., Kobayashi, S., Andrae, U., Balmaseda, M. A., Balsamo, G., Bauer, P., Bechtold, P., Beljaars, A. C. M., van de Berg, L., Bidlot, J., Bormann, N., Delsol, C., Dragani, R., Fuentes, M., Geer, A. J., Haimberger, L., Healy, S. B., Hersbach, H., Hólm, E. V., Isaksen, I., Kållberg, P., Köhler, M., Matricardi, M., McNally, A. P., Monge-Sanz, B. M., Morcrette, J.-J., Park, B.-K., Peubey, C., de Rosnay, P., Tavolato, C., Thépaut, J.-N., and Vitart, F.: The ERA-Interim reanalysis: configuration and performance of the data assimilation system, 137, 553-597, 10.1002/qj.828, 2011.
- 440 Dentener, F., Kinne, S., Bond, T., Boucher, O., Cofala, J., Generoso, S., Ginoux, P., Gong, S., Hoelzemann, J. J., Ito, A., Marelli, L., Penner, J. E., Putaud, J. P., Textor, C., Schulz, M., van der Werf, G. R., and Wilson, J.: Emissions of primary aerosol and precursor gases in the years 2000 and 1750 prescribed data-sets for AeroCom, *Atmos. Chem. Phys.*, 6, 4321-4344, 10.5194/acp-6-4321-2006, 2006.
- Dlugokencky, E. J., Myers, R. C., Lang, P. M., Masarie, K. A., Crotwell, A. M., Thoning, K. W., Hall, B. D., Elkins, J. W., and Steele, L. P.: Conversion of NOAA atmospheric dry air CH<sub>4</sub> mole fractions to a gravimetrically prepared standard scale, *Journal of Geophysical Research: Atmospheres*, 110, doi:10.1029/2005JD006035, 2005.
- 450 Doerr, S. H., and Santín, C.: Global trends in wildfire and its impacts: perceptions versus realities in a changing world, 371, 20150345, doi:10.1098/rstb.2015.0345, 2016.



- 455 Duncan, B., Yoshida, Y., R. Olson, J., Sillman, S., Martin, R., Lamsal, L., Hu, Y., E. Pickering, K., Retscher, C., and J. Allen, D.: Application of OMI observations to a space-based indicator of NO<sub>x</sub> and VOC controls on surface ozone formation, 2213-2223 pp., 2010.
- Edwards, J. M., and Slingo, A.: Studies with a flexible new radiation code. I: Choosing a configuration for a large-scale model, *Quarterly Journal of the Royal Meteorological Society*, 122, 689-719, 10.1002/qj.49712253107, 1996.
- 460 Etheridge, D. M., Steele, L. P., Francey, R. J., and Langenfelds, R. L.: Atmospheric methane between 1000 A.D. and present: Evidence of anthropogenic emissions and climatic variability, *Journal of Geophysical Research: Atmospheres*, 103, 15979-15993, doi:10.1029/98JD00923, 1998.
- Fels, S. B., Mahlman, J. D., Schwarzkopf, M. D., and Sinclair, R. W.: Stratospheric Sensitivity to Perturbations in Ozone and Carbon Dioxide: Radiative and Dynamical Response, 37, 2265-2297, 10.1175/1520-0469(1980)037<2265:Sstpio>2.0.Co;2, 1980.
- 465 Forster, P., and Shine, K. P.: Radiative forcing and temperature trends from stratospheric ozone changes, 102, 10841-10855, 10.1029/96jd03510, 1997.
- Gauss, M., Myhre, G., Isaksen, I. S. A., Grewe, V., Pitari, G., Wild, O., Collins, W. J., Dentener, F. J., Ellingsen, K., Gohar, L. K., Hauglustaine, D. A., Iachetti, D., Lamarque, F., Mancini, E., Mickley, L. J., Prather, M. J., Pyle, J. A., Sanderson, M. G., Shine, K. P., Stevenson, D. S., Sudo, K., Szopa, S., and Zeng, G.: Radiative forcing since preindustrial times due to ozone change in the troposphere and the lower stratosphere, *Atmos. Chem. Phys.*, 6, 575-599, 10.5194/acp-6-575-2006, 2006.
- 470 Giglio, L., Randerson, J. T., and van der Werf, G. R.: Analysis of daily, monthly, and annual burned area using the fourth-generation global fire emissions database (GFED4), 118, 317-328, 10.1002/jgrg.20042, 2013.
- Guenther, A. B., Jiang, X., Heald, C. L., Sakulyanontvittaya, T., Duhl, T., Emmons, L. K., and Wang, X.: The Model of Emissions of Gases and Aerosols from Nature version 2.1 (MEGAN2.1): an extended and updated framework for modeling biogenic emissions, *Geosci. Model Dev.*, 5, 1471-1492, 10.5194/gmd-5-1471-2012, 2012.
- 475 Hamilton, D. S., Hantson, S., Scott, C. E., Kaplan, J. O., Pringle, K. J., Nieradzik, L. P., Rap, A., Folberth, G. A., Spracklen, D. V., and Carslaw, K. S.: Reassessment of pre-industrial fire emissions strongly affects anthropogenic aerosol forcing, *Nature Communications*, 9, 3182, 10.1038/s41467-018-05592-9, 2018.
- Hantson, S., Knorr, W., Schurgers, G., Pugh, T. A. M., and Arneth, A.: Global isoprene and monoterpene emissions under changing climate, vegetation, CO<sub>2</sub> and land use, *Atmospheric Environment*, 155, 35-45, <https://doi.org/10.1016/j.atmosenv.2017.02.010>, 2017.
- 480 Hartmann, D. L., Klein Tank, A. M. G., Rusticucci, M., Alexander, L. V., Brönnimann, S., Charabi, Y., Dentener, F. J., Dlugokencky, E. J., Easterling, D. R., Kaplan, A., Soden, B. J., Thorne, P. W., Wild, M., and Zhai, P. M.: Observations: Atmosphere and Surface, in: *Climate Change 2013: The Physical Science Basis. Contribution of Working Group I to the Fifth Assessment Report of the Intergovernmental Panel on Climate Change*, edited by: Stocker, T. F., Qin, D., Plattner, G.-K., Tignor, M., Allen, S. K., Boschung, J., Nauels, A., Xia, Y., Bex, V., and Midgley, P. M., Cambridge University Press, Cambridge, United Kingdom and New York, NY, USA, 159-254, 2013.
- Hollaway, M. J., Arnold, S. R., Collins, W. J., Folberth, G., and Rap, A.: Sensitivity of midnineteenth century tropospheric ozone to atmospheric chemistry-vegetation interactions, 122, 2452-2473, 10.1002/2016jd025462, 2017.
- 490 Jian, Y., and Fu, T. M.: Injection heights of springtime biomass-burning plumes over peninsular Southeast Asia and their impacts on long-range pollutant transport, *Atmos. Chem. Phys.*, 14, 3977-3989, 10.5194/acp-14-3977-2014, 2014.
- Kapadia, Z. Z., Spracklen, D. V., Arnold, S. R., Borman, D. J., Mann, G. W., Pringle, K. J., Monks, S. A., Reddington, C. L., Benduhn, F., Rap, A., Scott, C. E., Butt, E. W., and Yoshioka, M.: Impacts of aviation fuel sulfur content on climate and human health, *Atmos. Chem. Phys.*, 16, 10521-10541, 10.5194/acp-16-10521-2016, 2016.
- 495 Kaplan, J. O., Krumhardt, K. M., Ellis, E. C., Ruddiman, W. F., Lemmen, C., and Goldewijk, K. K.: Holocene carbon emissions as a result of anthropogenic land cover change, *The Holocene*, 21, 775-791, 10.1177/0959683610386983, 2011.
- Klein Goldewijk, K., Beusen, A., van Drecht, G., and de Vos, M.: The HYDE 3.1 spatially explicit database of human-induced global land-use change over the past 12,000 years, *Global Ecology and Biogeography*, 20, 73-86, doi:10.1111/j.1466-8238.2010.00587.x, 2011.
- 500 Knorr, W., Kaminski, T., Arneth, A., and Weber, U.: Impact of human population density on fire frequency at the global scale, *Biogeosciences*, 11, 1085-1102, 10.5194/bg-11-1085-2014, 2014.
- Lamarque, J. F., Bond, T. C., Eyring, V., Granier, C., Heil, A., Klimont, Z., Lee, D., Liousse, C., Mieville, A., Owen, B., Schultz, M. G., Shindell, D., Smith, S. J., Stehfest, E., Van Aardenne, J., Cooper, O. R., Kainuma, M., Mahowald, N., McConnell, J. R., Naik, V., Riahi, K., and van Vuuren, D. P.: Historical (1850-2000) gridded anthropogenic and biomass burning emissions of reactive gases and aerosols: methodology and application, *Atmos. Chem. Phys.*, 10, 7017-7039, 10.5194/acp-10-7017-2010, 2010.
- 505 Laothawornkitkul, J., Taylor, J. E., Paul, N. D., and Hewitt, C. N.: Biogenic volatile organic compounds in the Earth system, 183, 27-51, 10.1111/j.1469-8137.2009.02859.x, 2009.
- Lathière, J., Hewitt, C. N., and Beerling, D. J.: Sensitivity of isoprene emissions from the terrestrial biosphere to 20th century changes in atmospheric CO<sub>2</sub> concentration, climate, and land use, 24, 10.1029/2009gb003548, 2010.
- 510 Lee, L. A., Pringle, K. J., Reddington, C. L., Mann, G. W., Stier, P., Spracklen, D. V., Pierce, J. R., and Carslaw, K. S.: The magnitude and causes of uncertainty in global model simulations of cloud condensation nuclei, *Atmos. Chem. Phys.*, 13, 8879-8914, 10.5194/acp-13-8879-2013, 2013.
- Lelieveld, J., and Dentener, F. J.: What controls tropospheric ozone?, 105, 3531-3551, 10.1029/1999jd901011, 2000.
- 515 Malik, T., Gajbhiye, T., and Pandey, S.: Seasonality in emission patterns of isoprene from two dominant tree species of Central India: Implications on terrestrial carbon emission and climate change, 8, 204-212, 2018.



- Mann, G., S. Carslaw, K., Spracklen, D., A. Ridley, D., T. Manktelow, P., Chipperfield, M., Pickering, S., and E. Johnson, C.: Description and evaluation of GLOMAP-mode: A modal global aerosol microphysics model for the UKCA composition-climate model, 2010.
- 520 Marlon, J. R., Bartlein, P. J., Carcaillet, C., Gavin, D. G., Harrison, S. P., Higuera, P. E., Joos, F., Power, M. J., and Prentice, I. C.: Climate and human influences on global biomass burning over the past two millennia, *Nature Geoscience*, 1, 697, 10.1038/ngeo313. <https://www.nature.com/articles/ngeo313#supplementary-information>, 2008.
- Marlon, J. R., Kelly, R., Daniau, A. L., Vanni re, B., Power, M. J., Bartlein, P., Higuera, P., Blarquez, O., Brewer, S., Br cher, T., Feurdean, A., Romera, G. G., Iglesias, V., Maezumi, S. Y., Magi, B., Courtney Mustaphi, C. J., and Zhihai, T.: Reconstructions of biomass burning from sediment-charcoal records to improve data–model comparisons, *Biogeosciences*, 13, 3225–3244, 10.5194/bg-13-3225-2016, 2016.
- 525 McNorton, J., Chipperfield, M., Gloor, M., Wilson, C., Wuhu, F., Hayman, G., Rigby, M., B. Krummel, P., O’Doherty, S., Prinn, R., Weiss, R., Young, D., Dlugokencky, E., and Montzka, S. A.: Role of OH variability in the stalling of the global atmospheric CH<sub>4</sub> growth rate from 1999 to 2006, 1–24 pp., 2016.
- 530 Mickley, L. J., Jacob, D. J., and Rind, D.: Uncertainty in preindustrial abundance of tropospheric ozone: Implications for radiative forcing calculations, 106, 3389–3399, 10.1029/2000jd900594, 2001.
- Monks, P. S., Archibald, A. T., Colette, A., Cooper, O., Coyle, M., Fowler, R., Fowler, D., Granier, C., Law, K. S., Mills, G. E., Stevenson, D. S., Tarasova, O., Thouret, V., von Schneidemesser, E., Sommariva, R., Wild, O., and Williams, M. L.: Tropospheric ozone and its precursors from the urban to the global scale from air quality to short-lived climate
- 535 forcer, *Atmos. Chem. Phys.*, 15, 8889–8973, 10.5194/acp-15-8889-2015, 2015.
- Monks, S., R. Arnold, S., Hollaway, M., Pope, R., Wilson, C., Wuhu, F., Emmerson, K., J. Kerridge, B., Latter, B., M. Miles, G., Siddans, R., and P. Chipperfield, M.: The TOMCAT global chemical transport model v1.6: Description of chemical mechanism and model evaluation, 3025–3057 pp., 2017.
- Murray, L. T., Mickley, L. J., Kaplan, J. O., Sofen, E. D., Pfeiffer, M., and Alexander, B.: Factors controlling variability in the oxidative capacity of the troposphere since the Last Glacial Maximum, *Atmos. Chem. Phys.*, 14, 3589–3622, 10.5194/acp-14-3589-2014, 2014.
- 540 Myhre, G., Shindell, D., Br on, F.-M., Collins, W., Fuglestedt, J., Huang, J., Koch, D., Lamarque, J.-F., Lee, D., Mendoza, B., Nakajima, T., Robock, A., Stephens, G., Takemura, T., and Zhang, H.: Anthropogenic and Natural Radiative Forcing, in: *Climate Change 2013: The Physical Science Basis. Contribution of Working Group I to the Fifth Assessment Report of the Intergovernmental Panel on Climate Change*, edited by: Stocker, T. F., Qin, D., Plattner, G.-K., Tignor, M., Allen, S. K., Boschung, J., Nauels, A., Xia, Y., Bex, V., and Midgley, P. M., Cambridge University Press, Cambridge, United Kingdom and New York, NY, USA, 659–740, 2013.
- Naik, V., Voulgarakis, A., Fiore, A. M., Horowitz, L. W., Lamarque, J. F., Lin, M., Prather, M. J., Young, P. J., Bergmann, D., Cameron-Smith, P. J., Cionni, I., Collins, W. J., Dalsg ren, S. B., Doherty, R., Eyring, V., Faluvegi, G., Folberth, G. A., Josse, B., Lee, Y. H., MacKenzie, I. A., Nagashima, T., van Noije, T. P. C., Plummer, D. A., Righi, M., Rumbold, S. T., Skeie, R., Shindell, D. T., Stevenson, D. S., Strode, S., Sudo, K., Szopa, S., and Zeng, G.: Preindustrial to present-day changes in tropospheric hydroxyl radical and methane lifetime from the Atmospheric Chemistry and Climate Model Intercomparison Project (ACCMIP), *Atmos. Chem. Phys.*, 13, 5277–5298, 10.5194/acp-13-5277-2013, 2013.
- 555 Pacifico, F., Folberth, G. A., Jones, C. D., Harrison, S. P., and Collins, W. J.: Sensitivity of biogenic isoprene emissions to past, present, and future environmental conditions and implications for atmospheric chemistry, 117, 10.1029/2012jd018276, 2012.
- Pfeiffer, M., Spessa, A., and Kaplan, J. O.: A model for global biomass burning in preindustrial time: LPJ-LMfire (v1.0), *Geosci. Model Dev.*, 6, 643–685, 10.5194/gmd-6-643-2013, 2013.
- 560 Rabin, S. S., Melton, J. R., Lasslop, G., Bachelet, D., Forrest, M., Hantson, S., Kaplan, J. O., Li, F., Mangeon, S., Ward, D. S., Yue, C., Arora, V. K., Hickler, T., Kloster, S., Knorr, W., Nieradzki, L., Spessa, A., Folberth, G. A., Sheehan, T., Voulgarakis, A., Kelley, D. I., Prentice, I. C., Sitch, S., Harrison, S., and Arneth, A.: The Fire Modeling Intercomparison Project (FireMIP), phase 1: experimental and analytical protocols with detailed model descriptions, *Geosci. Model Dev.*, 10, 1175–1197, 10.5194/gmd-10-1175-2017, 2017.
- 565 Randerson, J. T., Chen, Y., van der Werf, G. R., Rogers, B. M., and Morton, D. C.: Global burned area and biomass burning emissions from small fires, 117, 10.1029/2012jg002128, 2012.
- Randerson, J. T., Van Der Werf, G. R., Giglio, L., Collatz, G. J., and Kasibhatla, P. S.: Global Fire Emissions Database, Version 4.1 (GFEDv4), in: ORNL Distributed Active Archive Center, 2017.
- Rap, A., Richards, N. A. D., Forster, P. M., Monks, S. A., Arnold, S. R., and Chipperfield, M. P.: Satellite constraint on the tropospheric ozone radiative effect, *Geophysical Research Letters*, 42, 5074–5081, doi:10.1002/2015GL064037, 2015.
- 570 Rap, A., Scott, C. E., Reddington, C. L., Mercado, L., Ellis, R. J., Garraway, S., Evans, M. J., Beerling, D. J., MacKenzie, A. R., Hewitt, C. N., and Spracklen, D. V.: Enhanced global primary production by biogenic aerosol via diffuse radiation fertilization, *Nature Geoscience*, 11, 640–644, 10.1038/s41561-018-0208-3, 2018.
- Rowlinson, M. J., Rap, A., Arnold, S. R., Pope, R. J., Chipperfield, M. P., McNorton, J., Forster, P., Gordon, H., Pringle, K. J., Feng, W., Kerridge, B. J., Latter, B. L., and Siddans, R.: Impact of El Ni o–Southern Oscillation on the interannual variability of methane and tropospheric ozone, *Atmos. Chem. Phys.*, 19, 8669–8686, 10.5194/acp-19-8669-2019, 2019.
- 575 Rubino, M., D’Onofrio, A., Seki, O., and Bendle, J. A.: Ice-core records of biomass burning, *The Anthropocene Review*, 3, 140–162, 10.1177/2053019615605117, 2016.



- 580 Schurgers, G., Arneth, A., Holzinger, R., and Goldstein, A. H.: Process-based modelling of biogenic monoterpene emissions  
combining production and release from storage, *Atmos. Chem. Phys.*, 9, 3409-3423, 10.5194/acp-9-3409-2009, 2009.
- Scott, C. E., Monks, S. A., Spracklen, D. V., Arnold, S. R., Forster, P. M., Rap, A., Äijälä, M., Artaxo, P., Carslaw, K. S.,  
Chipperfield, M. P., Ehn, M., Gilardoni, S., Heikkinen, L., Kulmala, M., Petäjä, T., Reddington, C. L. S., Rizzo, L.  
V., Swietlicki, E., Vignati, E., and Wilson, C.: Impact on short-lived climate forcers increases projected warming due  
585 to deforestation, *Nature Communications*, 9, 157, 10.1038/s41467-017-02412-4, 2018.
- Shindell, D. T., Pechony, O., Voulgarakis, A., Faluvegi, G., Nazarenko, L., Lamarque, J. F., Bowman, K., Milly, G., Kovari,  
B., Ruedy, R., and Schmidt, G. A.: Interactive ozone and methane chemistry in GISS-E2 historical and future climate  
simulations, *Atmos. Chem. Phys.*, 13, 2653-2689, 10.5194/acp-13-2653-2013, 2013.
- Sindelarova, K., Granier, C., Bouarar, I., Guenther, A., Tilmes, S., Stavrou, T., Müller, J. F., Kuhn, U., Stefani, P., and  
590 Knorr, W.: Global data set of biogenic VOC emissions calculated by the MEGAN model over the last 30 years, *Atmos.  
Chem. Phys.*, 14, 9317-9341, 10.5194/acp-14-9317-2014, 2014.
- Singh, H. B.: Reactive nitrogen in the troposphere, *Environmental Science & Technology*, 21, 320-327, 10.1021/es00158a001,  
1987.
- Smith, B., Wärnlind, D., Arneth, A., Hickler, T., Leadley, P., Siltberg, J., and Zaehle, S.: Implications of incorporating N cycling  
595 and N limitations on primary production in an individual-based dynamic vegetation model, *Biogeosciences*, 11, 2027-  
2054, 10.5194/bg-11-2027-2014, 2014.
- Stevenson, D. S., Young, P. J., Naik, V., Lamarque, J. F., Shindell, D. T., Voulgarakis, A., Skeie, R. B., Dalsoren, S. B., Myhre,  
G., Bernsten, T. K., Folberth, G. A., Rumbold, S. T., Collins, W. J., MacKenzie, I. A., Doherty, R. M., Zeng, G., van  
Noije, T. P. C., Strunk, A., Bergmann, D., Cameron-Smith, P., Plummer, D. A., Strode, S. A., Horowitz, L., Lee, Y.  
H., Szopa, S., Sudo, K., Nagashima, T., Josse, B., Cionni, I., Righi, M., Eyring, V., Conley, A., Bowman, K. W.,  
600 Wild, O., and Archibald, A.: Tropospheric ozone changes, radiative forcing and attribution to emissions in the  
Atmospheric Chemistry and Climate Model Intercomparison Project (ACCMIP), *Atmos. Chem. Phys.*, 13, 3063-  
3085, 10.5194/acp-13-3063-2013, 2013.
- Swetnam, T. W., Farella, J., Roos, C. I., Liebmann, M. J., Falk, D. A., and Allen, C. D.: Multiscale perspectives of fire, climate  
605 and humans in western North America and the Jemez Mountains, USA, *Philosophical Transactions of the Royal  
Society B: Biological Sciences*, 371, 20150168, doi:10.1098/rstb.2015.0168, 2016.
- Unger, N.: Human land-use-driven reduction of forest volatiles cools global climate, *Nature Climate Change*, 4, 907,  
10.1038/nclimate2347. <https://www.nature.com/articles/nclimate2347#supplementary-information>, 2014.
- van der Werf, G. R., Randerson, J. T., Giglio, L., Collatz, G. J., Mu, M., Kasibhatla, P. S., Morton, D. C., DeFries, R. S., Jin,  
610 Y., and van Leeuwen, T. T.: Global fire emissions and the contribution of deforestation, savanna, forest, agricultural,  
and peat fires (1997–2009), *Atmos. Chem. Phys.*, 10, 11707-11735, 10.5194/acp-10-11707-2010, 2010.
- van der Werf, G. R., Peters, W., van Leeuwen, T. T., and Giglio, L.: What could have caused pre-industrial biomass burning  
emissions to exceed current rates?, *Clim. Past*, 9, 289-306, 10.5194/cp-9-289-2013, 2013.
- van Marle, M. J. E., Kloster, S., Magi, B. I., Marlon, J. R., Daniiau, A. L., Field, R. D., Arneth, A., Forrest, M., Hantson, S.,  
Kehrwald, N. M., Knorr, W., Lasslop, G., Li, F., Mangeon, S., Yue, C., Kaiser, J. W., and van der Werf, G. R.:  
615 Historic global biomass burning emissions for CMIP6 (BB4CMIP) based on merging satellite observations with  
proxies and fire models (1750–2015), *Geosci. Model Dev.*, 10, 3329-3357, 10.5194/gmd-10-3329-2017, 2017.
- Volz, A., and Kley, D.: Evaluation of the Montsouris series of ozone measurements made in the nineteenth century, *Nature*,  
332, 240-242, 10.1038/332240a0, 1988.
- 620 Voulgarakis, A., and Field, R. D.: Fire Influences on Atmospheric Composition, Air Quality and Climate, *Current Pollution  
Reports*, 1, 70-81, 10.1007/s40726-015-0007-z, 2015.
- Wang, Z., Chappellaz, J., Park, K., and Mak, J. E.: Large Variations in Southern Hemisphere Biomass Burning During the  
Last 650 Years, *Science*, 330, 1663-1666, 10.1126/science.1197257, 2010.
- Wild, O.: Modelling the global tropospheric ozone budget: exploring the variability in current models, *Atmos. Chem. Phys.*,  
625 7, 2643-2660, 10.5194/acp-7-2643-2007, 2007.
- Yeung, L. Y., Murray, L. T., Martinerie, P., Witrant, E., Hu, H., Banerjee, A., Orsi, A., and Chappellaz, J.: Isotopic constraint  
on the twentieth-century increase in tropospheric ozone, *Nature*, 570, 224-227, 10.1038/s41586-019-1277-1, 2019.
- Young, P. J., Archibald, A. T., Bowman, K. W., Lamarque, J. F., Naik, V., Stevenson, D. S., Tilmes, S., Voulgarakis, A., Wild,  
O., Bergmann, D., Cameron-Smith, P., Cionni, I., Collins, W. J., Dalsøren, S. B., Doherty, R. M., Eyring, V., Faluvegi,  
G., Horowitz, L. W., Josse, B., Lee, Y. H., MacKenzie, I. A., Nagashima, T., Plummer, D. A., Righi, M., Rumbold,  
630 S. T., Skeie, R. B., Shindell, D. T., Strode, S. A., Sudo, K., Szopa, S., and Zeng, G.: Pre-industrial to end 21st century  
projections of tropospheric ozone from the Atmospheric Chemistry and Climate Model Intercomparison Project  
(ACCMIP), *Atmos. Chem. Phys.*, 13, 2063-2090, 10.5194/acp-13-2063-2013, 2013.
- Zhu, L., Val Martin, M., Gatti, L. V., Kahn, R., Hecobian, A., and Fischer, E. V.: Development and implementation of a new  
635 biomass burning emissions injection height scheme (BBEIH v1.0) for the GEOS-Chem model (v9-01-01), *Geosci.  
Model Dev.*, 11, 4103-4116, 10.5194/gmd-11-4103-2018, 2018.